RESEARCH ARTICLE SUMMARY

DISEASE DYNAMICS

A transmissible cancer shifts from emergence to endemism in Tasmanian devils

Austin H. Patton, Matthew F. Lawrance, Mark J. Margres, Christopher P. Kozakiewicz, Rodrigo Hamede, Manuel Ruiz-Aravena, David G. Hamilton, Sebastien Comte, Lauren E. Ricci, Robyn L. Taylor, Tanja Stadler, Adam Leaché, Hamish McCallum, Menna E. Jones, Paul A. Hohenlohe, Andrew Storfer*

INTRODUCTION: Emerging infectious diseases pose one of the greatest threats to human health and biodiversity. Phylodynamics is an effective tool for inferring epidemiological parameters to guide intervention strategies, particularly for human viruses such as severe acute respiratory syndrome coronavirus 2 (SARS-CoV-2). However, phylodynamic analysis has historically been limited to the study of rapidly evolving viruses and, in rare cases, bacteria. Nonetheless, application of phylodynamics to nonviral pathogens has immense potential, such as for predicting disease spread and informing the management of wildlife diseases.

We conducted a phylodynamics analysis of devil facial tumor disease (DFTD), a transmissible cancer that has spread across nearly the entire geographic range of Tasmanian devils and threatens the species with extinction. DFTD is transmitted as an allograft through biting during common social interactions, susceptibility is nearly universal, and case fatality rates approach 100%. The goals of our study were to (i) characterize the geographic spread of DFTD, (ii) identify whether there are different circulating tumor lineages, and (iii) quantify rates of transmission among lineages.

RATIONALE: In principle, phylodynamics should be readily extended to the study of slowly evolving pathogens with large genomes through careful interrogation of genes to identify those that are measurably evolving. By testing individual genes for a clocklike signal, these genes may then be used for phylodynamic analysis. We demonstrate this proof of concept in DFTD.

RESULTS: We screened >11,000 genes across the DFTD genome, identifying 28 that exhibited a strong, clocklike signal, and performed the first phylodynamic analysis of a genome larger than a bacterium. We demonstrate here, contrary to field observations, that DFTD spread omnidirectionally throughout the epizootic, leaving little signal of geographic structuring of tumor lineages across Tasmania. Despite predictions of devil extinction, we found that the effective reproduction number (R_E), a summary of the rate at which disease spreads, has declined precipitously after the initial epidemic spread of DFTD. Specifically, R_E peaked at a high of ~3.5 shortly after the discovery of DFTD in 1996 and is now ~1 in both extant tumor lineages. This is consistent with a shift from emergence to endemism. Except for a single gene, we found little evidence for convergent molecular evolution among tumor lineages.

CONCLUSION: We have demonstrated that phylodynamics can be applied to virtually any pathogen. In doing so, we show that through careful interrogation of the pathogen genome, a measurably evolving set of genes can be identified to characterize epidemiological dynamics of nonviral pathogens with large genomes. By applying this approach to DFTD, we have shown that the disease appears to be transitioning from emergence to endemism. Consistent with recent models, our inference that R_E ~1 predicts that coexistence between devils and DFTD is a more likely outcome than devil extinction. Therefore, our findings present cautious optimism for the continued survival of the iconic Tasmanian devil but emphasize the need for evolutionarily informed conservation management to ensure their persistence. ■

PHOTOS: DAVID G. HAMILTON (TOP), ALEXANDRA K. FRAIK (BOTTOM).

Tasmanian devils and their transmissible cancer. Healthy (top) and DFTD-infected (bottom) Tasmanian devils.

The list of author affiliations is available in the full article online.
*Corresponding author. Email: astorfer@wsu.edu
Cite this article as: A. H. Patton *et al.*, *Science* **370**, eabb9772 (2020). DOI: 10.1126/science.abb9772

READ THE FULL ARTICLE AT
https://doi.org/10.1126/science.abb9772

RESEARCH ARTICLE

DISEASE DYNAMICS

A transmissible cancer shifts from emergence to endemism in Tasmanian devils

Austin H. Patton[1,2], Matthew F. Lawrance[1], Mark J. Margres[3], Christopher P. Kozakiewicz[1], Rodrigo Hamede[4,5], Manuel Ruiz-Aravena[4,6], David G. Hamilton[4], Sebastien Comte[4,7], Lauren E. Ricci[1,8], Robyn L. Taylor[4], Tanja Stadler[9,10], Adam Leaché[11], Hamish McCallum[7,12], Menna E. Jones[4], Paul A. Hohenlohe[13], Andrew Storfer[1]*

Emerging infectious diseases pose one of the greatest threats to human health and biodiversity. Phylodynamics is often used to infer epidemiological parameters essential for guiding intervention strategies for human viruses such as severe acute respiratory syndrome coronavirus 2 (SARS-Cov-2). Here, we applied phylodynamics to elucidate the epidemiological dynamics of Tasmanian devil facial tumor disease (DFTD), a fatal, transmissible cancer with a genome thousands of times larger than that of any virus. Despite prior predictions of devil extinction, transmission rates have declined precipitously from ~3.5 secondary infections per infected individual to ~1 at present. Thus, DFTD appears to be transitioning from emergence to endemism, lending hope for the continued survival of the endangered Tasmanian devil. More generally, our study demonstrates a new phylodynamic analytical framework that can be applied to virtually any pathogen.

Emerging infectious diseases (EIDs) threaten the health of wildlife, livestock, domestic animals, and humans (*1*). One of the primary contributors to species endangerment (*2*), EIDs have also led or contributed to notable extinctions, including dozens of amphibian species by chytridiomycosis (*3*), the Polynesian tree snail (*Partula turgida*) by a microsporidian infection (*4*), and 16 species of Hawaiian honeycreepers (Drepanidini, Fringillidae) by avian malaria (*Plasmodium relictum*) and avian pox [*Poxvirus avium* (*2*)]. EIDs also can have profound impacts on society; indeed, the emergence of severe acute respiratory syndrome coronavirus 2 (SARS-Cov-2) has led to socioeconomic consequences that will surely last for years to come (*5*).

[1]School of Biological Sciences, Washington State University, Pullman, WA 99164, USA. [2]Department of Integrative Biology and Museum of Vertebrate Zoology, University of California, Berkeley, CA 94720, USA. [3]Department of Integrative Biology, University of South Florida, Tampa, FL 33620, USA. [4]School of Biological Sciences, University of Tasmania, Hobart, Tasmania 7001, Australia. [5]CANECEV, Centre de Recherches Ecologiques et Evolutives sur le Cancer (CREEC), Montpellier 34090, France. [6]Department of Microbiology and Immunology, Montana State University, Bozeman, MT 59717, USA. [7]Vertebrate Pest Research Unit, Invasive Species and Biosecurity, NSW Department of Primary Industries, Orange, New South Wales 2800, Australia. [8]Department of Wildland Resources, Utah State University, Logan, UT 84322, USA. [9]Department for Biosystems Science and Engineering, ETH Zürich, Basel 4058, Switzerland. [10]Swiss Institute of Bioinformatics, 1015 Lausanne, Switzerland. [11]Department of Biology and Burke Museum of Natural History and Culture, University of Washington, Seattle, WA 98195, USA. [12]Environmental Futures Research Institute, Griffith University, Brisbane, Queensland 4111, Australia. [13]Department of Biological Science, University of Idaho, Moscow, ID 83844, USA.
*Corresponding author. Email: astorfer@wsu.edu

Recently, phylodynamics has emerged as an invaluable tool for the characterization of the epidemiological dynamics of such rapidly evolving pathogens (*6*, *7*). By reconstructing pathogen phylogenies, phylodynamic analyses elucidate critically relevant epidemiological parameters such as the effective reproduction number (R_E) (*8*) and the effective number of infections (N_E) (*9*). R_E is a generalization of the basic reproduction number (R_0) in epidemiological models, or the expected number of secondary infections from a single infected individual entering a wholly susceptible population. Similarly, R_E quantifies transmission in populations already infected, predicts when pathogen prevalence will increase ($R_E > 1$) or decrease ($R_E < 1$), and helps to estimate the vaccination fraction necessary to achieve herd immunity.

Although phylodynamics has contributed substantially to the management of human diseases, including the responses to SARS-Cov-2 (*10*), its application to nonviral pathogens such as bacteria has been limited by their slower rate of molecular evolution and larger genome sizes (*11*). Past efforts to apply phylodynamic approaches to pathogens other than viruses have been impeded by the challenges associated with large genome size and the identification of a measurably evolving portion of the pathogen genome with which to reconstruct phylogenies. However, the extension of phylodynamics to nonviral pathogens including many wildlife EIDs would prove invaluable for management and intervention.

A marquee example is Tasmanian devils (*Sarcophilus harrisii*; Fig. 1A), which are endangered by an unusual class of emerging infectious disease: a transmissible cancer (*12*). Devil facial tumor disease (DFTD; Fig. 1B) has spread across 95% of the devil's geographic range since its discovery in 1996, causing localized population declines exceeding 90% (*13*) and a species-wide decline of 80% (*12*, *14*). DFTD replicates clonally and is transmitted as an allograft through biting during social interactions (*15*). Case fatality rates are nearly 100%, and devil susceptibility appears to be largely universal (*12*) due in part to limited genetic variation caused by historical population bottlenecks (*16*).

Although efforts have been made to describe DFTD transmission dynamics early in the epizootic [e.g., (*17*)], little is known how its epidemiology has changed since emergence. Despite initial model predictions of devil extinction resulting from frequency-dependent transmission (*17*), populations persist even in long-diseased areas, and some populations may even be recovering (*14*, *18*). Clearly, more analyses are needed to reconcile the discrepancy between model predictions and empirical observations.

Herein, we characterized the epidemiological history of DFTD using whole-genome sequencing of 51 tumor samples selected to maximize spatiotemporal variation across Tasmania between 2003 and 2018 (fig. S1). By screening >11,000 genes distributed across the tumor genome, we identified a subset that is measurably evolving, thus demonstrating an approach that enables the application of a suite of phylodynamic methods to virtually any pathogen. We also dated the approximate emergence time of DFTD, determined the number of lineages present, tracked the rate and directionality of lineage spread, and estimated N_E and R_E.

Results

Identification of clocklike genes

We screened 11,359 total genes across the DFTD genome and identified 28 genes (totaling 431,608 bp) that were sufficiently variable (>50 parsimony-informative sites) and evolved at an appropriate clocklike manner for use in tip-dating our phylogeny (table S1). These 28 genes were distributed widely across the genome without any discernible pattern with respect to gene function. Once concatenated and aligned for the 51 final samples, the aligned matrix was composed of 431,608 total columns, 2520 parsimony-informative sites, 1893 singletons, 802 doubletons, and 2711 variants found in three or more individuals (fig. S2).

DFTD phylogeography

Using these 28 genes, we estimated the time of DFTD origination to be between 1977 and 1987 (mean = 1983.93; Fig. 1C and figs. S3, S7, and S8), which is compatible with its discovery in 1996 (*12*). Field studies indicate an origin of DFTD in northeastern Tasmania, with subsequent southern and westward spread across the

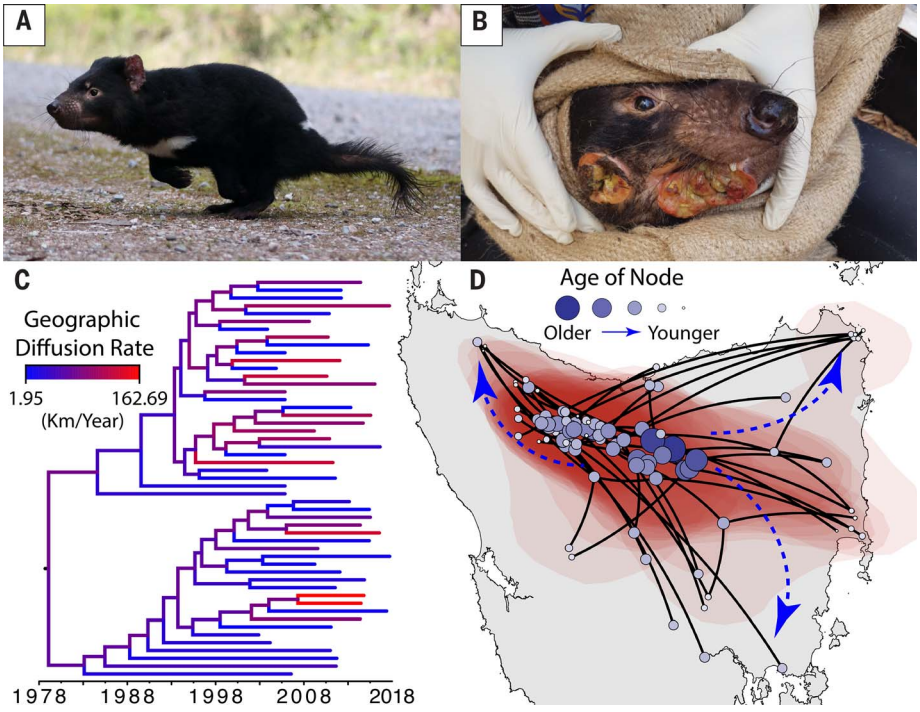

Fig. 1. Spread of DFTD lineages across Tasmania. (**A**) Healthy devil (Photo: David G. Hamilton). (**B**) Tasmanian devil infected with DFTD (Photo: Alexandra K. Fraik). (**C**) Phylogeny of 51 tumor samples; branch colors indicate the estimated geographic diffusion rate. Shown are branch lengths in units of time; the *x*-axis corresponds to year. (**D**) The same phylogeny mapped in geographic space. Blue circles correspond to both terminal and internal nodes, with size and color corresponding to age. Inferred locations of internal nodes correspond to our sampled lineages; no samples exist at the time and location of disease origination. Red polygons indicate posterior probability locations of historical infections. Dashed blue arrows indicate omnidirectional DFTD spread.

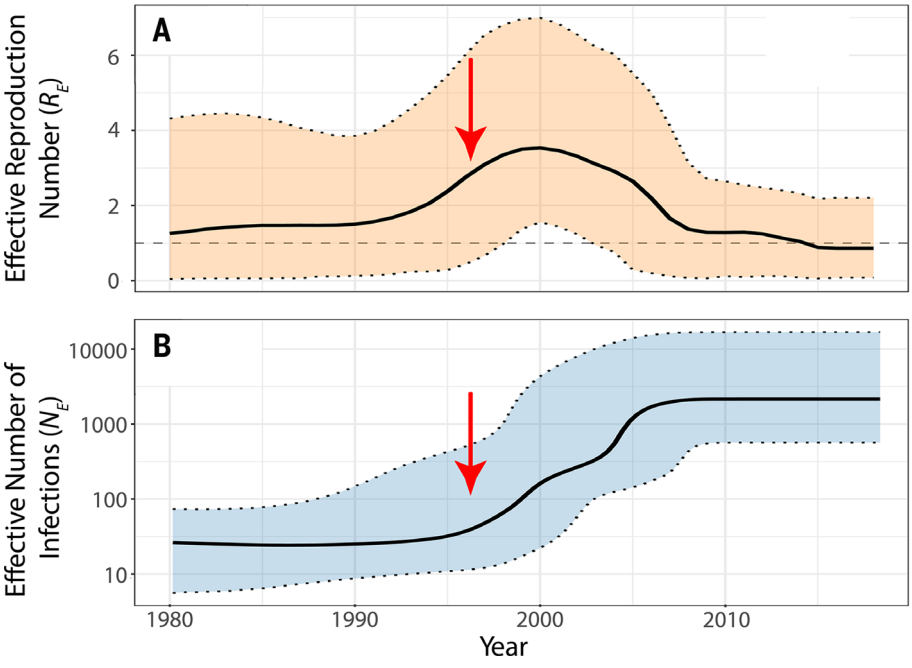

Fig. 2. Epidemiological dynamics of DFTD. Red arrows indicate the year of DFTD discovery (1996). Shading indicates the 95% credible intervals for parameter estimates; thick black lines are medians of the posterior distribution. (**A**) R_E through time under the birth-death skyline model. Dashed gray line indicates R_E = 1. Above this line, disease spreads; below it, the number of infections decreases. (**B**) N_E under the coalescent Bayesian skyline.

island (*13*). However, our phylogeographic reconstruction showed a more complex pattern of DFTD spread (Fig. 1D and movie S1). We found evidence for two contemporary, monophyletic DFTD lineages that emerged early in the epizootic and completely overlapped in their geographic distributions (Fig. 1, C and D), consistent with a recent landscape genetics study (*19*). After reaching central Tasmania, the cancer subsequently recolonized previously infected eastern and southern populations after their well-documented and extensive declines [e.g., (*13*, *14*)]. Our results suggest that the spread of DFTD continued omnidirectionally toward the present.

DFTD phylodynamics

Estimates of R_E through time are consistent with the discovery of DFTD in 1996; a low R_E at the time of disease origination would translate to low prevalence before discovery (Fig. 2A). The birth-death skyline, which assembles piecewise constant estimates of R_E, inferred a sudden, increased rate of transmission in the late 1990s (Fig. 2A). Specifically, R_E increased from ~1 around 1980 to a maximum of ~3.5. Currently R_E is <1, suggesting that DFTD will decrease in prevalence. The N_E (Fig. 2B) supports the same dynamics, showing a rapid increase in number of infections when R_E was >1, followed by a stabilization of the infected population size coinciding with an R_E of ~1.

The methods used above rely on the assumption that transmission dynamics do not vary among tumor lineages. Therefore, we relaxed these assumptions using a multistate birth-death model to determine whether tumor lineages differ in their epidemiological dynamics. We found that, indeed, transmission rate dynamics were not uniform across tumor lineages (Fig. 3A and fig. S9), with two detectable shifts in transmission rate. R_E (as estimated under the birth-death skyline) declined to just above or below 1 toward the present in each of the two, reciprocally monophyletic contemporary transmission clusters, respectively (Fig. 3B). Neither transmission cluster was geographically discrete; each was distributed island wide.

Genomic differentiation among transmission clusters

Our results show that accelerated transmission rates of DFTD began in the early to mid-1990s (Figs. 2A and 3B). With our data, we were unable to unequivocally determine what specifically led to this change. However, we screened the 51 tumor genomes and identified 791 unique variants that differentiated the three identified transmission clusters found in the top 0.1% of pF_{ST} (a measure of genomic differentiation) values. Of these variants, 687 were intergenic and the remaining 104 fell within a total of 68 unique genes and 70 unique transcripts (fig. S10).

These genes are associated with regulation of (i) STAT3 (NFATC3 and PRKG1), a key DFTD

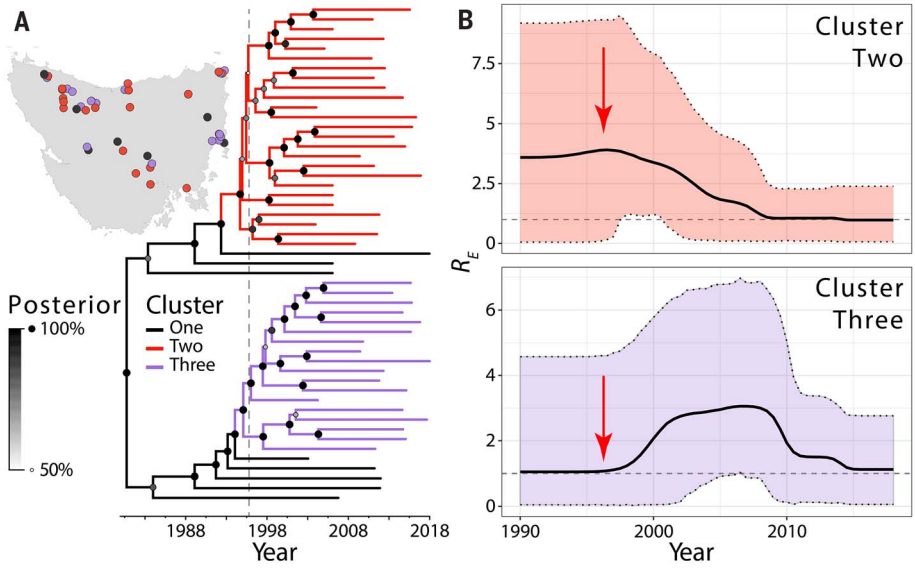

Fig. 3. Heterogeneous transmission rate dynamics in DFTD. (**A**) Phylogeny inferred under the birth-death skyline model. Branch colors show three distinct transmission rate regimes identified under the multistate birth-death model. Circles show posterior probability of interior nodes. Vertical dashed gray line indicates year of disease detection (1996). (**B**) Transmission rates through time as inferred under the birth-death skyline model for clusters 2 (red) and 3 (green). Median estimates are bold black lines; the 95% credible interval is shaded. Red arrows indicate the year of DFTD discovery (1996). Inset map shows the distribution of samples belonging to each transmission cluster, with points colored the same as in (A).

immune evasion protein (*20*); (ii) Schwann cell differentiation, the cell type of DFTD origin (*21*); and (iii) Wnt signaling (ARMC8, CDH17, DMXL1, and PKP2), a key process in cancer progression (*22*) and identified across previous DFTD genomic studies (*23*). The above genes were found to be highly differentiated between clusters 1 (black; Fig. 3A) and 3 (green), as well as between clusters 2 (red) and 3, but not between clusters 1 and 2.

Discussion

Herein, we have demonstrated that the phylodynamic analytical framework, although previously applied exclusively to viruses and a few bacteria, can be used to assess more slowly evolving pathogens with larger genomes. Through careful assessment of clocklike evolution across the genome, we were able to extract a measurably evolving signal across 28 genes totaling 431.6 kb. Note that this amount of sequence is far greater than that used in phylodynamic studies of viruses, including Ebola [~19.9 kb (*24*)], influenza A [13.6 kb (*25*)], and SARS-Cov-2 [~29.8 kb (*26*)]. Therefore, our approach can be readily applied to the study of other nonviral pathogens that previously fell outside of the scope of phylodynamic study. When applied to devil facial tumor disease, our analyses show (i) that DFTD originated well before its discovery in 1996; (ii) no geographic substructuring among two extant tumor lineages; (iii) omnidirectional spread of tumors; and (iv) a precipitous decline in transmission to replacement at present, indicating a shift to endemism.

Our study indicates that DFTD may have originated nearly a decade or more before its discovery in 1996. These findings are compatible with field observations; upon initial discovery in northeastern Tasmania, tumors were large and widespread in the population (*12*), so the disease had likely been circulating for some time. Nonetheless, it is possible that some host variants persisted in our multiple sequence alignments (MSAs) despite our best efforts to remove potential contamination (see the materials and methods). Because devil genomic variants will coalesce earlier than DFTD variants, a consequence of such contamination is that our inferred dates of disease origination are likely slightly earlier than the true origination date.

One surprising finding of our phylogeographic analysis was the apparent lack of geographical structuring of DFTD lineages. Rather, our results indicate that the disease spread omnidirectionally throughout the epizootic, repeatedly recolonizing previously infected populations that experienced substantial population declines [e.g., (*13*, *14*)]. That is, as devil populations reached low densities, they likely received infected migrant devils from neighboring areas, which is compatible with the observed disease-induced metapopulation dynamics (*27*) and local patterns of DFTD lineage replacement (*28*). Thus, our phylogeographic analysis challenges the conventional narrative of an east-to-west disease wave emanating from northeastern Tasmania (*12*) and instead suggests continuous spread in all cardinal directions (Fig. 1D).

These results differ slightly from those of Murchison *et al.* (*21*), who recovered evidence of fine-scale geographic structuring with the Forestier peninsula of southeastern Tasmania. Whereas we sampled 51 tumors across Tasmania between 2003 and 2018, 36 of the 68 tumor samples in Murchison *et al.* (*21*) came from the Forestier peninsula over a 4-year period. Additionally, the tumor phylogeny inferred by Murchison *et al.* (*21*) was based on 16 nuclear and 21 mitochondrial variants that were presumably somatic. By contrast, our phylogenies are based on 5406 total variants distributed across 28 measurably evolving genes.

Terminal branches of our inferred phylogenies are longer than internal branches, differing slightly from typical viral phylogenies. High within-host tumor diversity is one potential explanation, but evidence of this is limited and preliminary. The only study that compared within-host tumor variation found that only six tumors from 20 individuals could be distinguished. Furthermore, three of these six differed by only a single variant, thus demonstrating limited within-host variation (*21*) and the potential for superinfection by more than one tumor lineage.

An alternative explanation for long terminal branches comes from the widespread geographic distribution and complete geographic overlap of tumor lineages, which were also seen in (*19*). That is, because of the low-density sampling scheme of our study with respect to geographic and temporal distribution of samples, the probability of sampling two closely related samples at any time or place is low.

Although we infer a geographical origin in north-central Tasmania, this is likely due to the earliest DFTD samples being collected from this location. Note that this is not to be interpreted as the location at which DFTD originated because it is much more probable that the disease originated on the eastern coast, near the site of discovery (*12*). Our inference of the root location in central Tasmania is likely a consequence of the absence of samples collected at the general location and time of disease origin in northeastern Tasmania. Tissue samples of tumors were not collected until the early 2000s, so no samples exist from the time and location of disease origin. Further, the earliest available samples are from central Tasmania, not the site of disease origination. In turn, we view the reconstructed geographic root state as being the location of the most recent common ancestor of our samples rather than the location of disease origin.

We found three transmission clusters that differ in their epidemiological dynamics and have identified a number of genes that may contribute to the observed transmission rate

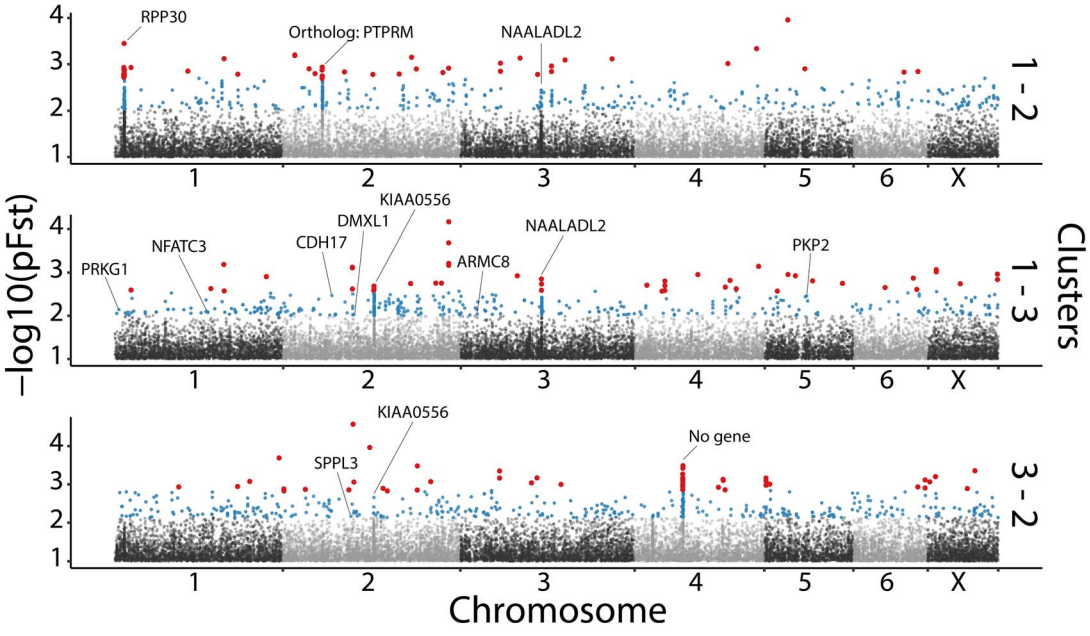

Fig. 4. Manhattan plot illustrating differentiation of SNPs in pairwise comparisons of transmission clusters using pF_{ST}. The top 0.1% most differentiated sites are shown in blue, and the top 0.01% most differentiated are shown in red. Select highly differentiated variants including those of functional importance are annotated. DFTD-associated genes discussed in the text are annotated.

variation. The absence of highly differentiated sites among clusters 1 and 2 could be caused by the minimal change in transmission rate at the time of origination of cluster 2 (Fig. 3B). These genes may thus contribute to the observed transmission rate variation and are candidates in need of further functional validation in vitro (Fig. 4 and tables S4 and S5).

Molecular evolution among DFTD transmission clusters could occur in two ways. In the first, convergent molecular evolution would be evidenced by the same genes becoming differentiated in each derived cluster (Fig. 3A). Alternatively, evolution could result in the differentiation of unique genes in each cluster. In general, each derived transmission cluster harbors a largely unique set of candidate SNPs, implicating unique mechanisms by which transmission rates vary. We only found a single gene (*NAALADL2*) consistent with the former (convergent) pattern of molecular evolution between clusters 2 and 3 (fig. S10 and table S4). This gene represents the only evidence recovered for potential convergent molecular evolution and may be important with respect to the oncogenicity of DFTD. *NAALADL2* has been demonstrated to be overexpressed in colon and prostate tumors compared with benign tumors in humans (*29*), and it promotes a tumor phenotype that exhibits greater capacity to migrate and metastasize. Future study of this gene in the context of DFTD evolution is thus warranted. Nonetheless, the observed transmission rate declines could be due to the accumulation of mutation load, which has been found in the canine transmissible cancer (*30*). Additionally, study of patterns of molecular evolution in the 28 clocklike genes identified in our study presents an exciting avenue of research.

Contrary to expectations of Tasmanian devil extinction (*13*, *17*), our results suggest that DFTD is transitioning from emergence to endemism. The large decline of R_E in the two pandemic tumor lineages suggests either coexistence or DFTD extinction, a result consistently supported by recent models and field data (*27*, *31*). This decrease in R_E may be a consequence of devil population declines, leading to fewer transmission opportunities. Current low R_E values are consistent with a reduced force of infection estimated using mark-recapture field data (*32*) and possible demographic recovery of some populations (*33*). Contemporary transmission dynamics may result in either the long-term coexistence of DFTD and devils or DFTD extinction, outcomes predicted by individual-based models (*32*). However, the potential for coexistence does not imply recovery of devils to pre-DFTD population sizes; current models predict persistent, substantially reduced devil densities (*31*).

Our results support the growing body of evidence that if DFTD continues to progress naturally, then devil extinction is unlikely. Therefore, we urge caution in the consideration of introductions of captive-bred devils to infected populations, a practice that has already been set into action (*34*). If reduced devil densities are contributing to reduced transmission rates (*27*), then an artificial increase of population densities through such introductions may be unwise. Further, introduction of disease-naïve devils may swamp adaptation to this new selective pressure (*35*). Instead, the preferred management option may be to allow natural evolution to occur and only introduce captive devils as a last resort if demographic rescue is urgently needed.

The existence of two widespread transmission clusters with unique epidemiological dynamics also suggests that mitigation strategies such as an oral bait vaccine (*36*) should account for this diversity. Unfortunately, a second, independently evolving transmissible cancer, DFT2, has been discovered in southeastern Tasmania (*37*) and may become a growing threat. Transmissible tumors may thus be commonplace throughout the evolutionary history of devils, but initial studies do not support this conclusion (*38*). Comparative phylodynamics of DFT2 and DFTD will be essential to understand their relative transmission dynamics. Our results suggest cautious optimism for the continued survival of the iconic Tasmanian devil but emphasize the need for evolutionarily informed management practices to ensure its persistence (*18*).

Materials and Methods

Sample collection

Tumor biopsies were not collected from Tasmanian devils until the early 2000s, corresponding to the time of our earliest samples. Samples from the University of Tasmania collection were obtained under University of Tasmania ethics approval A13326 and Washington State University institutional animal

care and use committee approval ASAF 6796. Tumor tissue biopsies were obtained using a 3-mm biopsy punch from wild devils and detailed field trapping protocols that have been previously described (*12*, *39*).

Early sampling efforts across Tasmania have historically been heterogeneous, with much of the effort being focused on collection at disease fronts. Therefore, we made a concerted effort to incorporate samples that maximized the available temporal range (2003 to 2018) and geographic distribution of samples available in the two largest sample repositories at the University of Tasmania and the Tasmanian Department of Primary Industries, Parks, Water and Entertainment, Tasmania, Australia. Where possible, samples were obtained such that the dataset represented the geographical distribution of DFTD in Tasmania through time, with the caveat that samples from eastern Tasmania are unavailable earliest in the collections, and collection has ceased at a number of sites in central Tasmania. Further, for devils that had tumor biopsies taken multiple times, we selected tumor biopsies that were associated with the first tumor biopsy for that devil.

Thus, in 2018 we obtained 50 tumor samples spread both geographically and temporally (2003 to 2018; fig. S1) across Tasmania. Whole-genomic libraries were prepared using NEB-next (New England Biolabs, Ipswitch, MA, USA) kits and sequenced on 26 lanes of a 10× Illumina Platform at Northwestern Genomics (Seattle, WA). An additional six whole-genome tumor samples originally sequenced for another study (*23*) were also included (BioProject PRJNA472767; BioSamples SAMN09242213, SAMN09242220, SAMN09242222, SAMN09242223, SAMN09242224, and SAMN09242226).

Sequencing read assembly

Raw reads were merged using flash2 (*40*) and adaptors trimmed with sickle (*41*). Trimmed reads were then aligned to the reference genome of *S. harrisii* (*21*) using bwa mem (*42*). Bam files produced from this step were subsequently sorted using Samtools (v1.9) sort (*43*). Samtools merge was then used to combine the sorted paired-end and single-end bam files for each sample; these combined bams were subsequently merged across lanes. Polymerase chain reaction duplicates were removed using Picard Markduplicates (*44*), and final bam files were indexed using the Samtools index.

Phylogenetic sequence preparation

To date, most phylodynamic studies have been conducted on extremely rapidly evolving viruses. Given that DFTD evolves much more slowly, we needed to ensure that the loci used to generate our phylogeny were measurably evolving. To accomplish this, we used an iterative approach that first identified a candidate set of genes evolving in a clocklike manner in both devils and tumors.

We first generated consensus sequences for the 22,391 annotated genes for the Tasmanian devil genome (Devil_ref v7.0, INSDC Assembly GCA_000189315.1). We generated consensus sequences for 48 of the 56 tumor isolates and 14 devil individuals using Samtools faidx. We then generated individual MSAs for 11,359 of the 22,391 genes using Clustal Omega (*45*). We only generated ~50% of the alignments because of computational constraints; these alignments took ~3 months to finish. However, the aligned genes were distributed across chromosomes 1 through 6, as well as the X chromosome, so we are not concerned that we are including a biased sample of the genome. We then summarized each alignment using AMAS (*46*), which quantifies the number of variable and parsimony-informative sites per gene.

Using these aligned genes, we subsequently inferred individual gene trees using IQ-TREE (*47*). Specifically, we fitted models of nucleotide substitution using the -m TEST flag, and the best-fit model was subsequently used for tree inference. We then tested, using each of the 11,359 gene trees, for a clocklike substitution process using the scripts provided by Murray *et al.* (*48*). These scripts regress phylogenetic root-to-tip distance against sampling date in a manner analogous to TempEst (*49*) to find the root branch that maximizes the fit of the regression. Significance was assessed by randomly permuting sampling dates across the tips 500 times, with the correlation coefficient as the test statistic.

We sought to identify a candidate set of genes that both exhibited a significant and realistic clocklike substitution process and harbored a sufficient number of phylogenetically informative sites to resolve the phylogeny. Therefore, we filtered these 11,359 genes such that only 364 were found to be evolving in a significant, clocklike manner ($P < 0.05$), harboring ≥50 parsimony sites, and with time to most recent common ancestor (MRCA) being inferred as <200 years before present (ybp). From this point forward, an additional eight tumor samples were included into our analyses, bringing the total number of sampled tumors to 56. These eight samples were previously excluded because of spontaneous regression [see (*23*)] but are included herein because we are specifically interested in broadscale patterns of transmission across Tasmania. The phylogenetic positions of these samples are indicated in fig. S3.

Next, we sought to remove single-nucleotide polymorphisms (SNPs) present in both devils and tumors, which would be indicative of potential host contamination in the tumor sample. To accomplish this, we called SNPs and indels for all 56 tumor samples using bcftools mpileup and bcftools call -mv. Indels were then normalized using bcftools norm -m. We then compared these SNPs and indels with those identified in the available 12 Tasmanian devil high-coverage (~30×) whole-genome sequences from Margres *et al.* (*35*) using bcftools isec to identify which SNPs and indels were unique to the tumor samples. We filtered out all variants shared between devils and tumors, leaving putatively somatic tumor variants that are not found as standing genetic variation in devil populations. This approach has been successfully applied to the study of DFTD recently (*50*) and is analogous to the approach used to study somatic variants in canine transmissible venereal tumor (*51*). Per-sample consensus sequences were then called using bcftools consensus in the manner described above.

We then inferred a final set of MSAs of all 56 tumor samples using MAFFT (*52*). Specifically, we ran MAFFT using the following settings: –local-pair –max-iterate 1000 and the accurate L-INS-I alignment method. We then repeated the workflow outlined above to infer gene trees using IQ-TREE, to test for clocklike signal, and to summarize alignments. As above, we subsequently filtered resultant MSAs such that only 28 genes were retained that were evolving in a significant ($P < 0.05$) clocklike manner, harboring >50 parsimony-informative sites, and exhibiting an MRCA < 200 ybp.

Phylodynamic inference

To expedite tree inference in our Bayesian phylodynamic analyses, we inferred a starting tree using concatenated sequences after automated model selection with IQ-TREE. We leveraged three complementary Bayesian phylodynamic methods in Beast v2.5.1 (*53*): Bayesian continuous phylogeography [visualized in SpreadD3 (*54*, *55*)], coalescent Bayesian skyline (*9*), and birth-death skyline (*8*) to: (i) characterize the phylogeographic history of DFTD as it spread across Tasmania, (ii) infer the demographic history of the disease, and (iii) quantify the rates of transmission throughout the epizootic. To test for among-lineage variation in transmission rates, we applied the multistate birth-death model (*56*), as implemented in R v3.6.1 (*57*), to the birth-death skyline maximum clade consensus tree. To quantify transmission rate variation in each cluster, we used the birth-death skyline model for the samples within each cluster. To prevent overfitting, we reduced the number of time series estimated R_E per cluster to five. We additionally used TreeTime (*58*) to conduct a root-to-tip regression of molecular divergence in the ML tree against time of sampling to obtain an estimate of the time of disease origination. Details specific to each analysis are described in the extended materials and methods in the supplementary materials.

Phylogenetic inference: Starting tree

As before, we implemented model selection in IQ-TREE on the concatenated sequence before topology inference. To quantify topological uncertainty, we conducted 100 rounds of bootstrapping. The ML tree was then read into TempEst to identify problematic sequences. We identified and removed five tumors that had outlying residuals or appeared to have mislabeled tip-dates. These five samples were excluded from all downstream analyses. In turn, we generated our final set of 51 tumor samples presented in the main text. After removal of these tumors, the inferred topology was subsequently visualized using FigTree (*59*).

Bayesian phylodynamic inference

For each of the Bayesian phylodynamic analyses described above, the best-fit model of nucleotide evolution as determined by IQ-TREE for the concatenated sequence was set in BEAST. Nondefault priors are shown in table S2. Four independent Markov chain Monte Carlo (MCMC) algorithms were run for 50 million generations, sampling every 1000 generations. Individual MCMC traces were compared to assess convergence using Tracer. Convergent chains were combined using LogCombiner, discarding the first 20% of samples for each chain as burn-in. Last, a single chain of 50 million generations was run, sampling from the prior only; these MCMC traces were used to assess deviation of the posterior from the prior for each estimated parameter. Maximum clade consensus trees from combined posterior distributions for each model were obtained using TreeAnnotater and visualized in FigTree.

Genomic differentiation among transmission clusters

To characterize genetic differences among transmission clusters identified under the multistate birth-death model, we identified SNPs in the genome exhibiting particularly strong differentiation among clusters, which are interpreted as candidates for the explanation of transmission rate variation using the pF_{ST} association test implemented in the GPAT++ software package (*60*, *61*). Specifically, we used this approach to identify candidate genomic variants that could explain the observed transmission rate variation. The pF_{ST} association test conducts a likelihood ratio test of allele frequency differences among populations, correcting for sequencing error using genotype likelihood scores in the calculation of model parameters. This approach has previously been successfully applied to the study of DFTD (*50*). To ensure that only confidently identified SNPs were retained in this analysis, we filtered the dataset using VCFtools v0.1.16 (*62*) using the following flags: –mac 4, –max-alleles 2, –min-alleles 2, –minDP 10, –max-missing 0.8, and –remove-indels. Specifically, we made all pairwise comparisons among identified transmission clusters and/or regimes. We subsequently characterized and extracted annotations from Ensembl for differentiated SNPs using the variant effect predictor (*63*).

REFERENCES AND NOTES

1. P. Daszak, A. A. Cunningham, A. D. Hyatt, Emerging infectious diseases of wildlife—Threats to biodiversity and human health. *Science* **287**, 443–449 (2000). doi: 10.1126/science.287.5452.443; pmid: 10642539
2. K. F. Smith, D. F. Sax, K. D. Lafferty, Evidence for the role of infectious disease in species extinction and endangerment. *Conserv. Biol.* **20**, 1349–1357 (2006). doi: 10.1111/j.1523-1739.2006.00524.x; pmid: 17002752
3. V. T. Vredenburg, R. A. Knapp, T. S. Tunstall, C. J. Briggs, Dynamics of an emerging disease drive large-scale amphibian population extinctions. *Proc. Natl. Acad. Sci. U.S.A.* **107**, 9689–9694 (2010). doi: 10.1073/pnas.0914111107; pmid: 20457913
4. A. A. Cunningham, P. Daszak, Extinction of a species of land snail due to infection with a microsporidian parasite. *Conserv. Biol.* **12**, 1139–1141 (1998). doi: 10.1046/j.1523-1739.1998.97485.x
5. I. Chakraborty, P. Maity, COVID-19 outbreak: Migration, effects on society, global environment and prevention. *Sci. Total Environ.* **728**, 138882 (2020). doi: 10.1016/j.scitotenv.2020.138882; pmid: 32335410
6. B. T. Grenfell *et al*., Unifying the epidemiological and evolutionary dynamics of pathogens. *Science* **303**, 327–332 (2004). doi: 10.1126/science.1090727; pmid: 14726583
7. E. M. Volz, K. Koelle, T. Bedford, Viral phylodynamics. *PLOS Comput. Biol.* **9**, e1002947 (2013). doi: 10.1371/journal.pcbi.1002947; pmid: 23555203
8. T. Stadler, D. Kühnert, S. Bonhoeffer, A. J. Drummond, Birth-death skyline plot reveals temporal changes of epidemic spread in HIV and hepatitis C virus (HCV). *Proc. Natl. Acad. Sci. U.S.A.* **110**, 228–233 (2013). doi: 10.1073/pnas.1207965110; pmid: 23248286
9. A. J. Drummond, A. Rambaut, B. Shapiro, O. G. Pybus, Bayesian coalescent inference of past population dynamics from molecular sequences. *Mol. Biol. Evol.* **22**, 1185–1192 (2005). doi: 10.1093/molbev/msi103; pmid: 15703244
10. S. M. Kissler, C. Tedijanto, E. Goldstein, Y. H. Grad, M. Lipsitch, Projecting the transmission dynamics of SARS-CoV-2 through the postpandemic period. *Science* **368**, 860–868 (2020). doi: 10.1126/science.abb5793; pmid: 32291278
11. R. Biek, O. G. Pybus, J. O. Lloyd-Smith, X. Didelot, Measurably evolving pathogens in the genomic era. *Trends Ecol. Evol.* **30**, 306–313 (2015). doi: 10.1016/j.tree.2015.03.009; pmid: 25887947
12. C. E. Hawkins *et al*., others, Emerging disease and population decline of an island endemic, the Tasmanian devil *Sarcophilus harrisii*. *Biol. Conserv.* **131**, 307–324 (2006). doi: 10.1016/j.biocon.2006.04.010
13. H. McCallum *et al*., Distribution and impacts of Tasmanian devil facial tumor disease. *EcoHealth* **4**, 318–325 (2007). doi: 10.1007/s10393-007-0118-0
14. B. T. Lazenby *et al*., Density trends and demographic signals uncover the long-term impact of transmissible cancer in Tasmanian devils. *J. Appl. Ecol.* **55**, 1368–1379 (2018). doi: 10.1111/1365-2664.13088; pmid: 30089931
15. A. M. Pearse, K. Swift, Allograft theory: Transmission of devil facial-tumour disease. *Nature* **439**, 549 (2006). doi: 10.1038/439549a; pmid: 16452970
16. A. H. Patton *et al*., Contemporary demographic reconstruction methods are robust to genome assembly quality: A case study in Tasmanian devils. *Mol. Biol. Evol.* **36**, 2906–2921 (2019). doi: 10.1093/molbev/msz191; pmid: 31424552
17. H. McCallum *et al*., Transmission dynamics of Tasmanian devil facial tumor disease may lead to disease-induced extinction. *Ecology* **90**, 3379–3392 (2009). doi: 10.1890/08-1763.1; pmid: 20120807
18. P. A. Hohenlohe *et al*., Conserving adaptive potential: Lessons from Tasmanian devils and their transmissible cancer. *Conserv. Genet.* **20**, 81–87 (2019). doi: 10.1007/s10592-019-01157-5; pmid: 31561664
19. C. P. Kozakiewicz *et al*., Comparative landscape genetics reveals differential effects of environment on host and pathogen genetic structure in Tasmanian devils (*Sarcophilus harrisii*) and their transmissible tumour. *Mol. Ecol.* **29**, 3217–3233 (2020). doi: 10.1111/mec.15558; pmid: 32682353
20. L. Kosack *et al*., The ERBB-STAT3 Axis Drives Tasmanian Devil Facial Tumor Disease. *Cancer Cell* **35**, 125–139.e9 (2019). doi: 10.1016/j.ccell.2018.11.018; pmid: 30645971
21. E. P. Murchison *et al*., Genome sequencing and analysis of the Tasmanian devil and its transmissible cancer. *Cell* **148**, 780–791 (2012). doi: 10.1016/j.cell.2011.11.065; pmid: 22341448
22. G. Davidson, C. Niehrs, Emerging links between CDK cell cycle regulators and Wnt signaling. *Trends Cell Biol.* **20**, 453–460 (2010). doi: 10.1016/j.tcb.2010.05.002; pmid: 20627573
23. M. J. Margres *et al*., The genomic basis of tumor regression in Tasmanian devils (*Sarcophilus harrisii*). *Genome Biol. Evol.* **10**, 3012–3025 (2018). pmid: 30321343
24. T. Wawina-Bokalanga *et al*., Complete genome sequence of a new Ebola virus strain isolated during the 2017 Likati outbreak in the Democratic Republic of the Congo. *Microbiol. Resour. Announc.* **8**, e00360-19 (2019). doi: 10.1128/MRA.00360-19; pmid: 31097506
25. G. Winter, S. Fields, Nucleotide sequence of human influenza A/PR/8/34 segment 2. *Nucleic Acids Res.* **10**, 2135–2143 (1982). doi: 10.1093/nar/10.6.2135; pmid: 6281731
26. A. Wu *et al*., Genome composition and divergence of the novel Coronavirus (2019-nCoV) originating in China. *Cell Host Microbe* **27**, 325–328 (2020). doi: 10.1016/j.chom.2020.02.001; pmid: 32035028
27. V. Siska, A. Eriksson, B. Mehlig, A. Manica, A metapopulation model of the spread of the Devil Facial Tumour Disease predicts the long term collapse of its host but not its extinction. bioRxiv 347062 [Preprint]. 14 June 2018. https://doi.org/10.1101/347062
28. R. K. Hamede *et al*., Transmissible cancer in Tasmanian devils: Localized lineage replacement and host population response. *Proc. Biol. Sci.* **282**, 20151468 (2015). doi: 10.1098/rspb.2015.1468; pmid: 26336167
29. H. C. Whitaker *et al*., N-acetyl-L-aspartyl-L-glutamate peptidase-like 2 is overexpressed in cancer and promotes a pro-migratory and pro-metastatic phenotype. *Oncogene* **33**, 5274–5287 (2014). doi: 10.1038/onc.2013.464; pmid: 24240687
30. P. W. Ewald, H. A. Swain Ewald, Infection and cancer in multicellular organisms. *Philos. Trans. R. Soc. Lond. B Biol. Sci.* **370**, 20140224 (2015). doi: 10.1098/rstb.2014.0224; pmid: 26056368
31. K. Wells *et al*., Individual and temporal variation in pathogen load predicts long-term impacts of an emerging infectious disease. *Ecology* **100**, e02613 (2019). doi: 10.1002/ecy.2613; pmid: 30636287
32. K. Wells *et al*., Infection of the fittest: Devil facial tumour disease has greatest effect on individuals with highest reproductive output. *Ecol. Lett.* **20**, 770–778 (2017). doi: 10.1111/ele.12776; pmid: 28489304
33. S. Comte, S. Carver, R. Hamede, M. Jones, Changes in spatial organization following an acute epizootic: Tasmanian devils and their transmissible cancer. *Glob. Ecol. Conserv.* **22**, e00993 (2020). doi: 10.1016/j.gecco.2020.e00993
34. S. Fox, P. J. Seddon, "Wild devil recovery: Managing devils in the presence of disease," in *Saving the Tasmanian Devil: Recovery Through Science-based Management*, C. Hogg, S. Fox, D. Pemberton, K. Belov, Eds. (CSIRO, 2019), pp. 157–164.
35. M. J. Margres *et al*., Large-effect loci affect survival in Tasmanian devils (*Sarcophilus harrisii*) infected with a transmissible cancer. *Mol. Ecol.* **27**, 4189–4199 (2018). doi: 10.1111/mec.14853; pmid: 30171778
36. A. S. Flies *et al*., An oral bait vaccination approach for the Tasmanian devil facial tumor diseases. *Expert Rev. Vaccines* **19**, 1–10 (2020). doi: 10.1080/14760584.2020.1711058; pmid: 31971036
37. R. J. Pye *et al*., A second transmissible cancer in Tasmanian devils. *Proc. Natl. Acad. Sci. U.S.A.* **113**, 374–379 (2016). doi: 10.1073/pnas.1519691113; pmid: 26711993
38. A. R. Stahlke, B. Epstein, S. Barbosa, A. Patton, S. A. Hendricks, A. Veillet, A. K. Fraik, B. Schönfeld, H. I. McCallum, R. Hamede, M. E. Jones, A. Storfer, P. A. Hohenlohe, Historical and contemporary signatures of selection in response to transmissible cancer in the Tasmanian devil (*Sarcophilus harrisii*). bioRxiv 241885 [Preprint]. 7 August 2020. https://doi.org/10.1101/2020.08.07.241885
39. R. K. Hamede, H. McCallum, M. Jones, Biting injuries and transmission of Tasmanian devil facial tumour disease. *J. Anim. Ecol.* **82**, 182–190 (2013). doi: 10.1111/j.1365-2656.2012.02025.x; pmid: 22943286
40. T. Magoč, S. L. Salzberg, FLASH: Fast length adjustment of short reads to improve genome assemblies. *Bioinformatics* **27**,

2957–2963 (2011). doi: 10.1093/bioinformatics/btr507; pmid: 21903629
41. N. A. Joshi, J. N. Fass, Sickle: a sliding-window, adaptive, quality-based trimming tool for FastQ files (2011); https://github.com/najoshi/sickle.
42. H. Li, Aligning sequence reads, clone sequences and assembly contigs with BWA-MEM. arXiv:1303.3997 [q-bio.GN] (26 May 2013).
43. H. Li *et al*., The Sequence Alignment/Map format and SAMtools. *Bioinformatics* **25**, 2078–2079 (2009). doi: 10.1093/bioinformatics/btp352; pmid: 19505943
44. Broad Institute, "Picard tools" (Broad Institute, 2018); http://broadinstitute.github.io/picard/.
45. F. Sievers, D. G. Higgins, Clustal Omega, accurate alignment of very large numbers of sequences. *Methods Mol. Biol.* **1079**, 105–116 (2014). doi: 10.1007/978-1-62703-646-7_6; pmid: 24170397
46. M. L. Borowiec, AMAS: A fast tool for alignment manipulation and computing of summary statistics. *PeerJ* **4**, e1660 (2016). doi: 10.7717/peerj.1660; pmid: 26835189
47. L.-T. Nguyen, H. A. Schmidt, A. von Haeseler, B. Q. Minh, IQ-TREE: A fast and effective stochastic algorithm for estimating maximum-likelihood phylogenies. *Mol. Biol. Evol.* **32**, 268–274 (2015). doi: 10.1093/molbev/msu300; pmid: 25371430
48. G. G. R. Murray *et al*., The effect of genetic structure on molecular dating and tests for temporal signal. *Methods Ecol. Evol.* **7**, 80–89 (2016). doi: 10.1111/2041-210X.12466; pmid: 27110344
49. A. Rambaut, T. T. Lam, L. Max Carvalho, O. G. Pybus, Exploring the temporal structure of heterochronous sequences using TempEst (formerly Path-O-Gen). *Virus Evol.* **2**, vew007 (2016). doi: 10.1093/ve/vew007; pmid: 27774300
50. M. J. Margres *et al*., Spontaneous tumor regression in Tasmanian devils associated with RASL11A activation. *Genetics* **215**, 1143–1152 (2020). doi: 10.1534/genetics.120.303428; pmid: 32554701
51. B. Decker *et al*., Comparison against 186 canid whole-genome sequences reveals survival strategies of an ancient clonally transmissible canine tumor. *Genome Res.* **25**, 1646–1655 (2015). doi: 10.1101/gr.190314.115; pmid: 26232412
52. K. Katoh, D. M. Standley, MAFFT multiple sequence alignment software version 7: Improvements in performance and usability. *Mol. Biol. Evol.* **30**, 772–780 (2013). doi: 10.1093/molbev/mst010; pmid: 23329690
53. R. Bouckaert *et al*., BEAST 2: A software platform for Bayesian evolutionary analysis. *PLOS Comput. Biol.* **10**, e1003537 (2014). doi: 10.1371/journal.pcbi.1003537; pmid: 24722319
54. P. Lemey, A. Rambaut, J. J. Welch, M. A. Suchard, Phylogeography takes a relaxed random walk in continuous space and time. *Mol. Biol. Evol.* **27**, 1877–1885 (2010). doi: 10.1093/molbev/msq067; pmid: 20203288
55. F. Bielejec *et al*., SpreaD3: Interactive visualization of spatiotemporal history and trait evolutionary processes. *Mol. Biol. Evol.* **33**, 2167–2169 (2016). doi: 10.1093/molbev/msw082; pmid: 27189542
56. J. Barido-Sottani, T. G. Vaughan, T. Stadler, Detection of HIV transmission clusters from phylogenetic trees using a multi-state birth-death model. *J. R. Soc. Interface* **15**, 20180512 (2018). doi: 10.1098/rsif.2018.0512; pmid: 30185544
57. R Core Team, "R: A language and environment for statistical computing" (R Foundation for Statistical Computing, 2019); www.R-project.org.
58. P. Sagulenko, V. Puller, R. A. Neher, TreeTime: Maximum-likelihood phylodynamic analysis. *Virus Evol.* **4**, vex042 (2018). doi: 10.1093/ve/vex042; pmid: 29340210
59. A. Rambaut, FigTree (2018), (available at http://tree.bio.ed.ac.uk/software/figtree/).
60. E. Garrison, "vcflib: C++ library and cmdline tools for parsing and manipulating VCF files" (2012); https://github.com/vcflib/vcflib.
61. Z. Kronenberg, M. D. Shapiro, "Association testing with GPAT++" (2014); https://github.com/zeeev/vcflib/wiki/Association-testing-with-GPAT.
62. P. Danecek *et al*., The variant call format and VCFtools. *Bioinformatics* **27**, 2156–2158 (2011). doi: 10.1093/bioinformatics/btr330; pmid: 21653522
63. W. McLaren *et al*., The Ensembl Variant Effect Predictor. *Genome Biol.* **17**, 122 (2016). doi: 10.1186/s13059-016-0974-4; pmid: 27268795
64. M. A. Suchard *et al*., Bayesian phylogenetic and phylodynamic data integration using BEAST 1.10. *Virus Evol.* **4**, vey016 (2018). doi: 10.1093/ve/vey016; pmid: 29942656
65. G. Baele, P. Lemey, Bayesian evolutionary model testing in the phylogenomics era: Matching model complexity with computational efficiency. *Bioinformatics* **29**, 1970–1979 (2013). doi: 10.1093/bioinformatics/btt340; pmid: 23766415
66. V. N. Minin, E. W. Bloomquist, M. A. Suchard, Smooth skyride through a rough skyline: Bayesian coalescent-based inference of population dynamics. *Mol. Biol. Evol.* **25**, 1459–1471 (2008). doi: 10.1093/molbev/msn090; pmid: 18408232
67. O. G. Pybus, A. Rambaut, P. H. Harvey, An integrated framework for the inference of viral population history from reconstructed genealogies. *Genetics* **155**, 1429–1437 (2000). pmid: 10880500
68. K. Strimmer, O. G. Pybus, Exploring the demographic history of DNA sequences using the generalized skyline plot. *Mol. Biol. Evol.* **18**, 2298–2305 (2001). doi: 10.1093/oxfordjournals.molbev.a003776; pmid: 11719579

ACKNOWLEDGMENTS

We thank L. Harmon, R. Gomulkiewicz, J. Kelley, O. Cornejo, A. Stalhke, and S. Barbosa for insightful discussions and recommendations. **Funding:** This work was funded by NIH grant no. R01-GM126563 as part of the NIH-NSF-USDA Ecology and Evolution of Infectious Diseases Program (to A.S., M.E.J., H.M., and P.A.H.) and by ARC DECRA grant no. DE170101116 (to R.H.). The research presented in this study was performed under University of Tasmania ethics approval A13326 and WSU IACUC approval ASAF 6796. **Author contributions:** A.H.P. conducted all analyses after the assembly of raw reads. M.L. extracted genomic DNA, assembled reads, and assisted in initial multiple sequence alignments. R.H., M.R.-A., D.G.H., S.C., and M.J. collected tumor biopsies. A.H.P. and A.S. wrote the manuscript with contributions from all other authors. H.M., M.J., P.A.H., and A.S. initially conceived of the project and all other authors contributed to its development. **Competing interests:** The authors declare no competing interests. **Data and materials availability:** Newly generated assembled sequence data are available from the NCBI Sequence Read Archive (SRA) under BioProject PRJNA613730, BioSample Accessions SAMN14418888-906, SAMN14418908-910, SAMN14418912, SAMN14418914-931, and SAMN15869204-7. All other supporting data and code are available in the supplementary materials.

SUPPLEMENTARY MATERIALS

science.sciencemag.org/content/370/6522/eabb9772/suppl/DC1
Materials and Methods
Supplementary Text
Figs. S1 to S11
Tables S1 to S5
References (*64*–*68*)
Movie S1
MDAR Reproducibility Checklist

30 March 2020; accepted 21 October 2020
10.1126/science.abb9772

A transmissible cancer shifts from emergence to endemism in Tasmanian devils

Austin H. Patton, Matthew F. Lawrance, Mark J. Margres, Christopher P. Kozakiewicz, Rodrigo Hamede, Manuel Ruiz-Aravena, David G. Hamilton, Sebastien Comte, Lauren E. Ricci, Robyn L. Taylor, Tanja Stadler, Adam Leach, Hamish McCallum, Menna E. Jones, Paul A. Hohenlohe, and Andrew Storfer

Science, **370** (6522), eabb9772.
DOI: 10.1126/science.abb9772

Emergence to endemism

The emergence of a devastating transmissible facial cancer among Tasmanian devils over the past few decades has caused substantial concern for their future because these animals are already threatened by a regional distribution and other stressors. Little is known about the overall history and trajectory of this disease. Patton *et al.* used an epidemiological phylodynamic approach to reveal the pattern of disease emergence and spread. They found that low Tasmanian devil densities appear to be contributing to slower disease growth and spread, which is good news for Tasmanian devil persistence and suggests that care should be taken when considering options for increasing devil populations.

Science, this issue p. eabb9772